Applied Catalysis A: General 493 (2015) 149–157

Contents lists available at ScienceDirect

Applied Catalysis A: General

journal homepage: www.elsevier.com/locate/apcata

Zirconia catalysts (ZrO_2 and Na-ZrO_2) for the conversion of phenethyl phenyl ether (PPE) in supercritical water

Hee-Jun Eom [a], Min-Sung Kim [a], Dae-Won Lee [a,*], Yoon-Ki Hong [a], Gwangsik Jeong [a], Kwan-Young Lee [a,b,**]

[a] Department of Chemical and Biological Engineering, Korea University, 145, Anam-ro, Seongbuk-gu, Seoul 136-701, Republic of Korea
[b] Green School, Korea University, 145, Anam-ro, Seongbuk-gu, Seoul 136-701, Republic of Korea

ARTICLE INFO

Article history:
Received 2 September 2014
Received in revised form 3 November 2014
Accepted 31 December 2014
Available online 8 January 2015

Keywords:
Lignin
β-Ether bond
Phenethyl phenyl ether
Na-ZrO_2
Supercritical water

ABSTRACT

In this study, the mesoporous ZrO_2 and Na-ZrO_2 were examined as heterogeneous solid catalysts under supercritical water for the *β-ether* bond scission of phenethyl phenyl ether (PPE). Na-ZrO_2 was more efficient than ZrO_2 in the dissociation of PPE. Yields of phenol and styrene were 39% and 16%, respectively, under 97% PPE conversion when 2.5 wt.% of Na-ZrO_2 catalyst was applied to a batch reactor filled with supercritical water (400 °C, 20 bar H_2 (initial pressure)) containing 2.5 wt.% PPE. The characterization revealed that the activities of ZrO_2 and Na-ZrO_2 were closely associated with the textural and acid/base properties of the catalysts. Notably, the reaction pathway and product distribution were determined by the concentration of acid and base sites on the catalyst's surface.

1. Introduction

Lignin is the aromatic polymers which are cross-linked with carbohydrates (cellulose and hemicellulose) to form lignocellulose [1]. Lignin has several biological functions. The most noted one is to provide the plant cell with hydrolytic resistance and chemical robustness [2–4]. As a biomass resource, lignin is important because it is the second most abundant organic polymer on Earth, constituting 30% of the non-fossil organic carbons on Earth [5,6]. Most importantly, on the basis of carbon neutrality and enormous availability, lignin is anticipated to become the most promising alternative resource for aromatic chemicals [7]. However, a major obstacle in valorizing lignin is its chemical stability, which is borne of its rigidly cross-linked structure. Using conventional reaction methods, it is very difficult to effectively decompose lignin into value-added aromatics [8]. Hydrolysis under high-temperature water (near or super-critical water) is known to be an effective strategy to decompose lignin [8,9].

Lignin is composed of hydroxyphenylpropane units (*p*-coumaryl, coniferyl and sinapyl alcohols), which are connected through various carbon–carbon and carbon–oxygen (ether) bonds [7,10]. Among the chemical linkages in lignin, the *β-ether* bond predominates, comprising 45–50% of the chemical linkages in softwood lignin and approximately 60% in hardwood lignin [7]. Because ether bonds are generally weaker than carbon–carbon bonds in chemical strength, lignin dissociation starts with *β-ether* bond cleavage [11]. Thus, it is meaningful to find catalysts that are active under high-temperature water for the cleavage of the *β-ether* bonds in lignin [12].

Meanwhile, the structure of lignin is complex and lacks a defined primary structure. Thus, lignin composition differs from sample to sample, making it difficult to obtain consistent reaction data when using lignin as the actual reactant. In such cases, it is more desirable to use a model substrate than to use lignin itself. If the purpose is to investigate the dissociation of the *β-ether* bond, phenethyl phenyl ether (PPE) is a good surrogate for lignin because it does not have unnecessary side chains around the *β-ether* bond and the hydrolysis products are comparatively accessible. The use of PPE as a model reactant for lignin was verified in several studies [13–15].

In our previous study, we investigated the dissociation of the *β-ether* bond in PPE under near/super-critical water supplemented with basic salt (Na_2CO_3) as a catalyst. The reaction is classified as homogeneous catalysis. The addition of sodium carbonate noticeably improved PPE conversion and resulted in the primary

* Corresponding author. Tel.: +82 2 3290 3299; fax: +82 2 926 6102.
** Corresponding author at: Department of Chemical and Biological Engineering, Korea University, 145, Anam-ro, Seongbuk-gu, Seoul 136-701, Republic of Korea. Tel.: +82 2 3290 3299; fax: +82 2 926 6102.
E-mail addresses: stayheavy@korea.ac.kr (D.-W. Lee), kylee@korea.ac.kr (K.-Y. Lee).

http://dx.doi.org/10.1016/j.apcata.2014.12.052
0926-860X/

production of phenol. It was postulated that phenol was produced *via* multiple routes that could be divided largely into two pathways: heterolytic *β-ether* bond cleavage and *α-hydrogen* abstraction of the Na^+-PPE intermediate [16]. In principle, heterogeneous catalysis is preferred over homogeneous catalysis because the latter requires additional costs due to catalyst recovery and waste treatment, which account for approximately 30% of the entire processing cost on average [17]. Moreover, the use of water-soluble catalyst bears a risk that the metallic salt may precipitate in supercritical water as solid particles, depending on the salt concentration and temperature [18]. Thus, our next step was verifying the feasibility of heterogeneous (solid) catalysis to dissociate lignin's *β-ether* bonds (PPE) under high-temperature water. Under high-temperature water conditions, PPE becomes miscible with water, forming a single-phase reactant, which is advantageous to heterogeneous catalysis as much as to homogeneous one in that it relieves mass transfer resistance at the catalyst-reactant interface.

Zirconia (ZrO_2) is an amphoteric solid widely used to catalyze various types of acid- and base-catalyzed reactions [19,20]. Zirconia-based materials perform well as catalysts when applied to the reactions involving H_2O and CO_2 specifically, because the acid and base sites of zirconia are not poisoned by H_2O and CO_2 [19,21,22]. The basic properties of ZrO_2 could be enhanced easily by incorporating an external component such as Na^+ [17], CaO [23], TiO_2 [24], *etc.* Additionally, ZrO_2 shows good chemical, mechanical and thermal stability, which makes it useful for a wide range of industrial catalytic applications.

ZrO_2 exists in three types of polymorphs: monoclinic, tetragonal, and cubic phases [25,26]. The tetragonal ZrO_2 is known to catalyze C—C bond cracking/formation reactions such as isomerization of *n*-butane [27] and benzylation of toluene [28]. The tetragonal ZrO_2 is thermodynamically stable at 1170–2370 °C. At lower temperatures, it is possible for ZrO_2 to exist in a metastable tetragonal phase; however, it is transformed into a monoclinic phase when temperatures reach higher than 400 °C. The transformation can be prevented with an alkaline solution post-treatment method, which is also known to improve the thermal stability [29,30], specific surface area [29,30] and base catalytic activity [17] of tetragonal zirconia. Liu et al. reported that when a zirconia gel is refluxed under aqueous NaOH solution for a sufficient time, Na^+ ions are incorporated into the zirconia framework, slowing down the rate of crystallization of zirconia during calcination and inhibiting the transition from the tetragonal to the monoclinic phase [17]. The net result is the stabilization of the specific surface area [17,31]. Such effects were valid at temperatures up to 800 °C [17]. Additionally, it was reported that the NaOH treatment generates strong basic sites by dispersing Na_2O nanocrystals over the zirconia framework.

In this study, mesoporous ZrO_2 catalysts post-treated with NaOH solution were applied in the hydrolysis of PPE under hydrogen-pressurized supercritical water. There are several published papers which studied the use of solid catalysts for the degradation (gasification) of lignin under near or super-critical water conditions [32,33]. However, to the best of our knowledge, no study has been reported yet, which deals with *β-ether* bond cleavage of PPE under high-temperature water using solid ZrO_2-based catalysts, with a purpose to obtain insights for heterogeneous catalytic dissociation of lignin.

To elucidate the compositional, crystallographic, textural and acid/base properties of the prepared catalysts, various characterization techniques were adopted, including inductively coupled plasma-atomic emission spectrometry (ICP-AES), low and wide angle X-ray diffraction (XRD), Brunauer–Emmett–Teller (BET) analysis, transmission electron microscopy (TEM), Fourier transform-infrared spectroscopy (FT-IR), carbon dioxide-temperature programmed desorption (CO_2-TPD) and ammonia-temperature programmed desorption (NH_3-TPD).

Correlating the reaction results with the properties of catalyst was attempted, and the reaction mechanisms were proposed based of those correlations.

2. Experimental

2.1. Materials

Phenethyl phenyl ether (99%) was purchased from Frinton Laboratories Inc. Poly(ethylene oxide)-poly(propylene oxide)-poly(ethylene oxide) (Aldrich, $PEO_{20}PPO_{70}PEO_{20}$, Pluronic P123), zirconium (IV) *n*-propoxide (Aldrich, 70 wt.% solution in 1-propanol), acetyl acetone (Aldrich, >99%), sodium hydroxide (Aldrich, 98%), and ethanol (J. T. Baker, HPLC grade) were used to prepare the catalysts. Water was purified to a resistivity of ≥18.2 MΩ/cm using an AquaMax-Ultra water purification system (Younglin). The gas chromatography mass spectrometry (GC–MS) spectra of phenol (Aldrich, >99%), toluene (Aldrich, >99.9%), ethylbenzene (Aldrich, >99%), and styrene (Aldrich, >99%) authentic standards were used to calibrate the GC signals of the products. Tetrahydrofuran (Aldrich, HPLC grade) was used as the recovery solvent without further purification.

2.2. Preparation of the zirconia catalysts

The synthesis of ZrO_2 catalysts was based on the method of Liu et al. [17]. First, 7.0 g of Pluronic P123 was dissolved in 140 mL of ethanol upon stirring. Then, 14 g of zirconium (IV) *n*-propoxide (70 wt.% solution in 1-propanol) was separately mixed with 1.5 g of acetylacetone while stirring. The two solutions were mixed together under vigorous stirring for 1 h at room temperature. Then, 5.4 g of deionized water was dropped (20 ml/h) into the solution, and the stirring was continued for 1 h. The mixture was gelated in a closed vessel at 60 °C for 48 h and then evaporated in a rotary evaporator (100 °C) under reduced pressure. The resulting transparent gel was refluxed under 0.5 mol/L NaOH aqueous solution for 48 h. Then, the slurry was washed thoroughly with deionized water until NaOH was completely removed. NaOH removal was confirmed with a pH meter. Finally, the resulting solid products were dried at 100 °C for 24 h and calcined at 500 °C for 5 h (ramping rate: 1 °C/min).

The prepared catalysts were named Na-ZrO_2 or ZrO_2 in accordance with whether the catalyst was refluxed under an aqueous solution of NaOH.

2.3. Characterization of catalysts

FT-IR analysis was performed with a Spectrum GX FTIR spectrometer (PerkinElmer Inc.) to determine if the residual surfactant (Pluronic P123) remained in the final form of the catalyst. The samples were diluted to 1 wt.% in KBr powder and then pelletized. The spectrum was recorded by co-adding 64 spectra in the range of 4000–370 cm^{-1} (resolution of 4 cm^{-1}) on a deuterated triglycine sulfate (DTGS) detector.

The Na content of the Na-ZrO_2 catalyst was determined by ICP-AES on an ULTIMA 2C HR instrument (Jobin Yvon Horiba). The measurement was conducted at the Korea Basic Science Institute (Seoul Center).

The specific surface areas of the catalysts were measured by the BET method on an ASAP 2010 instrument (Micromeritics). Before measurement, the sample (200 mg) was degassed at 300 °C and 4 mmHg for 12 h. The nitrogen adsorption–desorption isotherms were measured at −196 °C. The pore size distributions of catalysts were obtained by applying the Barrett–Joyner–Halenda (BJH) method to the adsorption branch of the isotherms.

Wide-angle XRD analysis was performed at room temperature on a D/MAX-2500 V/PC instrument (Rigaku). The X-ray source was

Ni-filtered Cu-Kα radiation (λ = 0.15418 nm), which was activated at 40 kV and 150 mA. The data were collected in the 2θ range from 20° to 70° with a scanning rate of 1°/min. The zirconia diffraction peaks were assigned by referring to the JCPDS database, PDF #42-1164 (tetragonal ZrO_2) and #83-0943 (monoclinic ZrO_2). The volume fraction (V_m) of the monoclinic phase was determined by applying the following Eq. (1) to the wide-angle XRD data [34].

$$V_m = \frac{1.311 \times X_m}{1 + 0.311 \times X_m}, \quad (1)$$

$$\text{where } X_m = \frac{I_m(1'\,1\,1) + I_m(1\,1\,1)}{I_m(1'\,1\,1) + I_m(1\,1\,1) + I_t(1\,0\,1)}$$

I_m (1′ 1 1) and I_m (1 1 1) are the intensities of the monoclinic ZrO_2 phase peaks, which appeared at 2θ = 28.1° and 31.4°, respectively. I_t (1 0 1) is the intensity of the tetragonal phase peak, which appeared at 2θ = 30.1°.

The crystallite size of the catalysts was determined by the *Scherrer* equation, which is given below.

$$\tau = \frac{K\lambda}{\beta \cos\theta} \quad (2)$$

τ: mean crystal size; *K*: constant (0.9); λ: X-ray wavelength (1.5406 Å); β: peak width (full width at half maximum, FWHM); θ: diffraction angle.

Low-angle XRD patterns were obtained on the same instrument. The data were collected in the 2θ range from 0.2° to 6° with a scanning rate of 0.2°/min.

CO_2 and NH_3-TPD analyses were performed on a BELCAT-M-77 instrument (BEL Japan Inc.), which was equipped with a thermal conductivity detector (TCD). The detailed procedures of the CO_2-TPD and NH_3-TPD experiments were as follows: the catalyst (200 mg) was enclosed in a quartz tube and heated at a rate of 10 °C/min to 500 °C, where the temperature was maintained for 2 h with flowing pure He at 40 ml/min. In CO_2-TPD, the sample was cooled down to 30 °C; CO_2 was adsorbed on the catalyst with flowing 5% CO_2/He gas at a rate of 35 ml/min. In NH_3-TPD, NH_3 was adsorbed at 100 °C using 5% NH_3/He gas (35 ml/min). Next, the catalyst was cooled down to room temperature under pure He flow (35 ml/min). The helium flow was maintained for 1 h to purge any excess CO_2 or NH_3 remaining on the catalyst surface. Finally, the TCD signal was recorded by elevating the temperature to 800 °C at a rate of 10 °C/min under pure He flow (35 ml/min). Desorption of CO_2 or NH_3 was quantified using the TCD calibration curve obtained by injecting CO_2 or NH_3 pulses of known volumes to a helium background flow.

FT-IR spectra of adsorbed pyridine were obtained on a Spectrum GX FTIR spectrometer (PerkinElmer Inc.). A catalyst powder was pressed into a self-supported wafer, which was loaded onto a sample holder and evacuated at 300 °C for 2 h. Then, it was cooled down to 150 °C and followed by exposure to pyridine vapor for 30 min. Physisorbed pyridine was removed by evacuation for 15 min. The spectrum was recorded by co-adding 128 spectra in the range of 1400–1700 cm^{-1} at a resolution of 4 cm^{-1}.

Catalyst morphology was investigated using TEM (Tecnai G2 20, FEI Company) operated at 200 kV. The sample was prepared by dispersing a catalyst powder over ethanol under ultrasonication for 30 min. The sample was spread on the carbon-coated copper grid (300 mesh) and dried at 80 °C for 1 h.

2.4. Reaction test

Reaction tests were performed in a 5 cm^3 stainless-steel-tube (SUS 316) bomb reactor. The reactor was equipped with a safety valve to release the high-pressure gas after the reaction was complete.

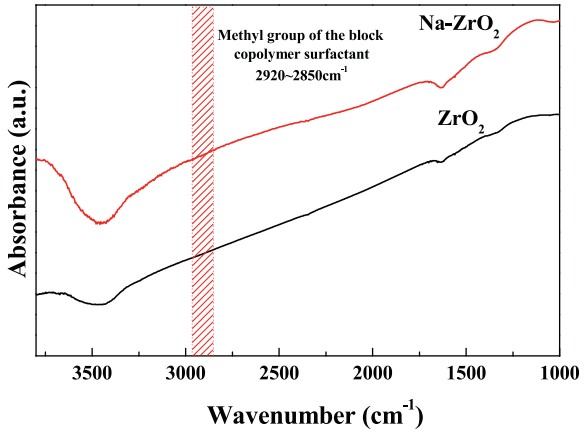

Fig. 1. FT-IR spectra of ZrO_2 and Na-ZrO_2 catalysts.

The reactor was loaded with 4 cm^3 of deionized water containing 2.5 wt.% of PPE and 2.5 wt.% of the solid catalyst. The reactor was filled with pure hydrogen gas, which was pressurized to 20 bar using a hydrogen gas booster (Hydromag Inc., HAG-AGD-32-P-T500). The reactor was placed into the pre-heated electric furnace and brought to the reaction temperature (400 °C) for 20 min. Approximately 2–3% of the PPE reacted during this heat-up time. This fraction was so small that it was neglected in evaluating the results of the reaction. The starting point of the reaction was defined by when the temperature reached 400 °C. After reaching that temperature, the reactor was shaken using a seesaw-type mechanical device. After the test, the reaction was quickly quenched by immersing the reactor in a cold-water bath at room temperature. The slurry inside the reactor was rinsed with tetrahydrofuran (THF) at a volume of 12 cm^3. The solids were separated from the liquid (THF) phase with filter paper. The products and (unreacted) reactant in the liquid phase were identified and quantified using GC–MS (Agilent 6890 GC coupled with 5973N mass selective detector, column: Restek, Rxi-5Sil MS, 30 m × 0.25 mm × 0.25 μm) analysis. In all cases, the gaseous products were minor and most reaction products were condensed in the liquid phase.

PPE conversion and product yields were calculated using the formula given below:

$$\text{PPE conversion}\,(\%) = \left(1 - \frac{\text{moles of PPE remained}}{\text{moles of PPE supplied}}\right) \times 100$$

$$\text{Product yield}\,(\%) = \frac{\text{moles of PPE remained}}{\text{moles of PPE supplied}} \times \frac{\text{carbon number of target product}}{\text{carbon number of PPE}} \times 100$$

Conversions and yields were evaluated three times and the average value was taken as the final result. The margin of error for the evaluation was within ±3.2%.

3. Results and discussion

3.1. Catalyst characterization

ICP-AES analysis showed that Na-ZrO_2 catalyst contained approximately 1.7 wt.% sodium.

Fig. 1 presents the FT-IR spectra of ZrO_2 and Na-ZrO_2. The CH_3, CH_2, and CH bands of the surfactant molecule (Pluronic P123), theoretically located at 2920, 2922, and 2850 cm^{-1}, respectively [35], were not observed in the spectra. This result implies that most

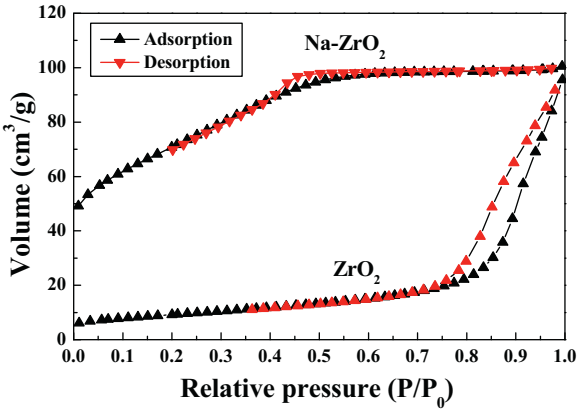

Fig. 2. Nitrogen adsorption–desorption isotherms of ZrO_2 (*fresh*) and Na-ZrO_2 (*fresh and used*) catalysts.

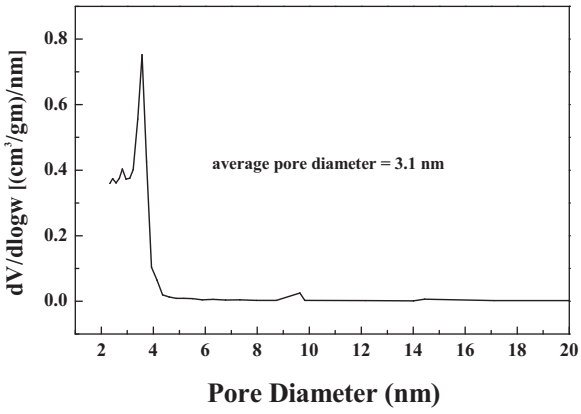

Fig. 3. Pore size distribution of Na-ZrO_2 catalyst (BJH method).

surfactant molecules were removed during the washing and calcination steps.

The textural properties of zirconia catalysts were analyzed by BET, low-angle XRD, and TEM analyses. Fig. 2 shows the nitrogen adsorption–desorption isotherms of the zirconia catalysts. The Na-ZrO_2 isotherm could be classified as a type IV isotherm, which is typical of mesoporous materials. Unlike Na-ZrO_2, ZrO_2 exhibited a type III isotherm, which is typical of non-porous or macroporous materials. In terms of specific surface area (Table 1), Na-ZrO_2 (157.0 $m^2\,g^{-1}$) was approximately 2 times larger than ZrO_2 (86 $m^2\,g^{-1}$). The pore size distribution of Na-ZrO_2 is presented in Fig. 3; the average pore size was estimated to be 3.1 nm. The low-angle XRD result for Na-ZrO_2 showed a distinct diffraction peak at $2\theta \fallingdotseq 1.4^\circ$ (Fig. 4), which confirmed the mesopore-scale ordering of crystallites in the catalyst. In contrast, the low-angle XRD result of ZrO_2 did not display a peak, implying that the mesoporous structure collapsed upon removal of the surfactant molecules during calcination [17]. The mesopore structure of the Na-ZrO_2 catalyst was captured in the TEM images, which showed wormhole-like pore channels that were very similar to those of mesoporous zirconia in other studies (Fig. 5) [17,36,37]. The images also showed

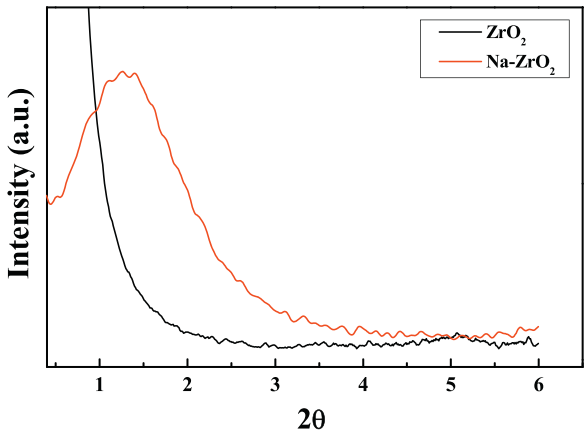

Fig. 4. Low-angle XRD patterns of ZrO_2 (*fresh*) and Na-ZrO_2 (*fresh and used*) catalysts.

that Na-ZrO_2 was much smaller in crystallite size than ZrO_2. It was supposed that incorporating sodium ions into the zirconia framework slowed zirconia's crystallization rate [17]. The results proved that the post-treatment with aqueous NaOH solution stabilized the mesoporous structure of zirconia, thereby resulting in a specific surface area higher than that of untreated zirconia. Meanwhile, the specific surface area of ZrO_2 catalyst drastically decreased by 58% (from 86.0 to 36.3 $m^2\,g^{-1}$) after the reaction test under supercritical water (Table 1). In comparison, Na-ZrO_2 showed a smaller decrease (20%) in specific surface area (from 157.0 to 121.6 $m^2\,g^{-1}$) after reaction test. The decrease of specific surface area might be due to the thermal growth of zirconia crystallites, which will be discussed later (in XRD data). The result matches well with the well-known fact that the incorporated Na^+ retards the thermal agglomeration of zirconia crystallites [17].

The results of the wide-angle XRD analysis are presented in Fig. 6. Na-ZrO_2 consisted of a pure tetragonal zirconia phase, while the untreated ZrO_2 was a mixture of tetragonal and monoclinic phases. In the untreated ZrO_2, the volume fraction of the monoclinic phase (V_m) was calculated as 95.4%, implying that most of the tetragonal phase was transformed into the monoclinic phase upon calcination at 500 °C. This result directly confirms that the tetragonal-to-monoclinic transition can be slowed by applying the aqueous NaOH solution post-treatment. The crystallite sizes, estimated by applying the Scherrer equation to the highest diffraction peaks (ZrO_2: t(1 0 1); Na-ZrO_2: m(1 1 1)), were 5.4 and 15.1 nm for Na-ZrO_2 and ZrO_2, respectively. This result matches well with the TEM analysis result (Fig. 5), which previously confirmed the decrease of crystallite size due to NaOH solution post-treatment.

The influence of basic solution treatment on the thermal growth of sol–gel-synthesized zirconia was well explained by Liu et al. [37]. It is suspected that the addition of basic solution induces the complete cross-linking of Zr—O groups in the gel, thereby turning the gel is into a homogeneously distributed, quasi nuclei state. The quasi-nuclei state facilitates crystallization at low temperatures. Thus, crystallization of the zirconia gel is nearly complete under the confinement of surfactant molecules before reaching the calcination temperature. As a result, the crystallization proceeds at a mild rate

Table 1
BET results of ZrO_2 (*fresh and used*) and Na-ZrO_2 (*fresh and used*) catalysts. The "*used*" means the catalyst recovered after reaction test.

Catalyst	Specific surface area, S_{BET} ($m^2\,g^{-1}$)	Total pore volume, V_p ($cm^3\,g^{-1}$)	Average pore size D_{BJH} (nm)
ZrO_2 (*fresh*)	86.0	0.06	3.1
ZrO_2 (*used*)	36.3	0.06	5.4
Na-ZrO_2 (*fresh*)	157.0	0.10	3.0
Na-ZrO_2 (*used*)	121.6	0.12	3.9

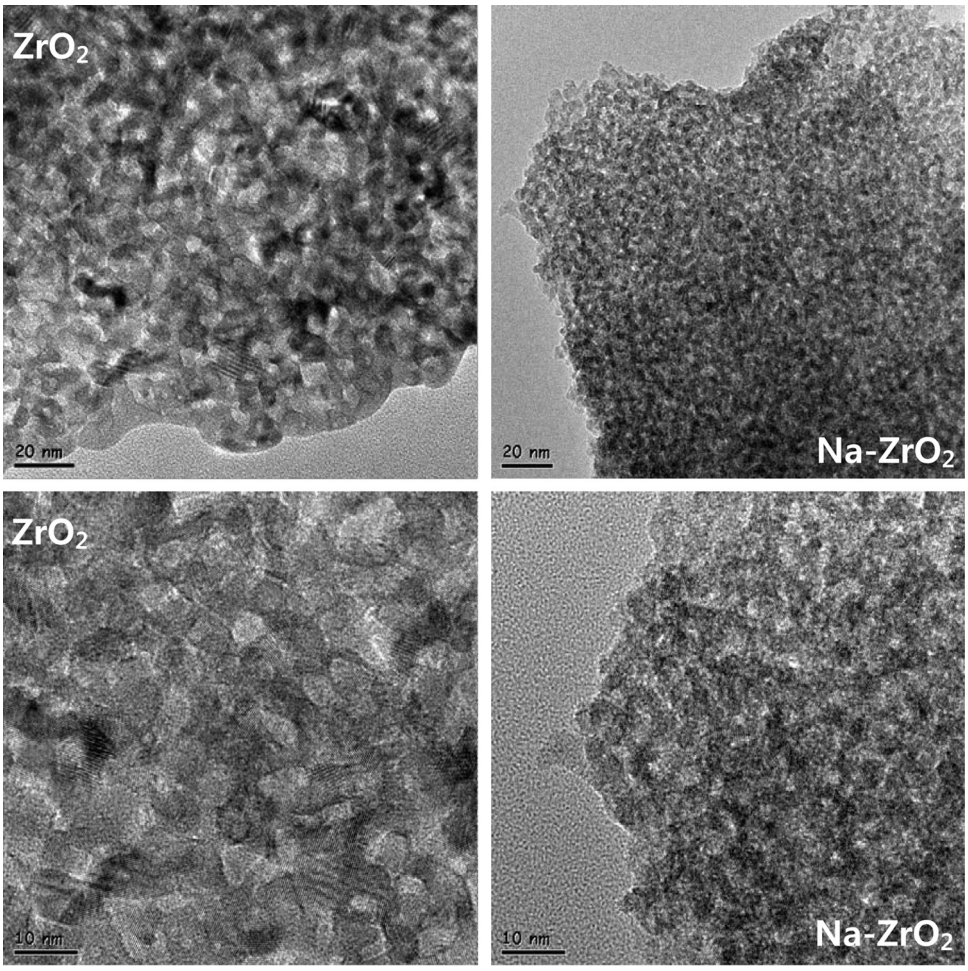

Fig. 5. TEM images of the ZrO_2 (*right*) and Na-ZrO_2 (*left*) catalysts.

when the calcination temperature is reached and maintained. The crystallites' thermal growth is slowed consequently.

CO_2-TPD analysis was performed to measure the strength and number of base sites present in the catalysts. The results are presented in Fig. 7. Based on literature values, the CO_2 peaks of zirconia were assigned as follows: CO_2 release at 25–180 °C is due to the decomposition of bidentate bicarbonate (*b*-HCO_3^-) and polydentate carbonate (*p*-CO_3^{2-}) adsorbed on *weak base sites*; the peak at 170–250 °C is due to the decomposition of bidentate carbonate (*b*-CO_3^{2-}) adsorbed on *medium strength base sites*; the peak at >230 °C is due to the decomposition of monodentate carbonate (*m*-CO_3^{2-}) adsorbed on *strong base sites* [38]. As seen in the figure, the weak and medium strength base sites were noticeably increased with the NaOH solution post-treatment. The increase of strong base sites was also observed but not as prominent as reported in the literature [17]. Na-ZrO_2 (3.58 mmol CO_2 g^{-1}) had 4 times as many base sites as ZrO_2 (0.86 mmol CO_2 g^{-1}) (Table 3). The discrepancy was smaller when normalizing for the difference in specific surface area between the catalysts: The area-specific base site density of Na-ZrO_2 (19.2 μmol CO_2 m^{-2}) was slightly higher than that of ZrO_2

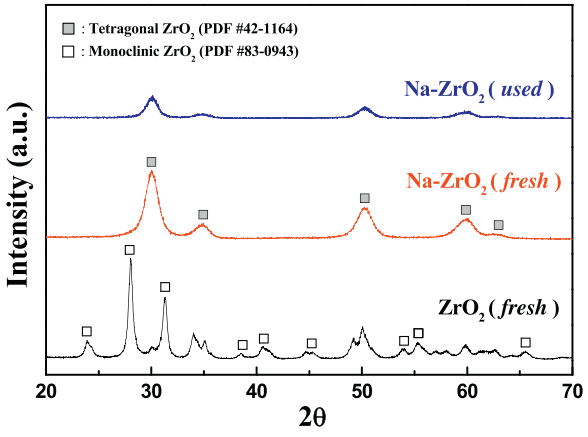

Fig. 6. Wide-angle XRD patterns of ZrO_2 and Na-ZrO_2 catalysts.

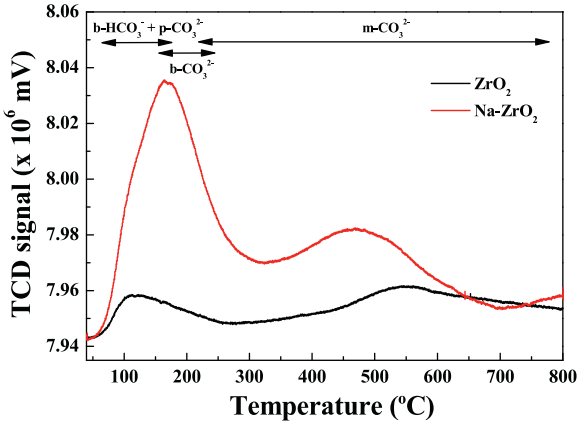

Fig. 7. CO_2-TPD profiles of ZrO_2 and Na-ZrO_2 catalysts.

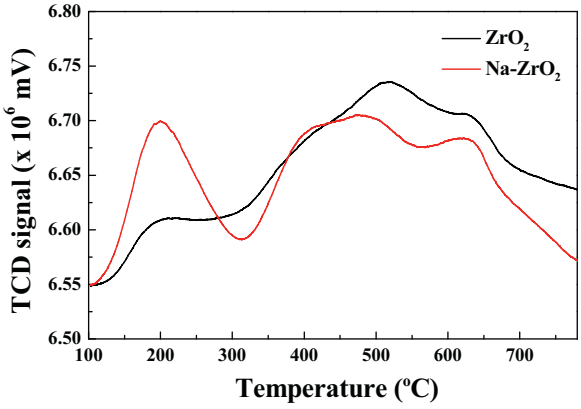

Fig. 8. NH_3-TPD profiles of ZrO_2 and Na-ZrO_2 catalysts.

(14.7 μmol CO_2 m^{-2}) (Table 3). Therefore, the enhanced specific surface area may be the primary reason for the increasing number of base sites (in weak and medium strength, especially) on the Na-ZrO_2 catalyst.

Zirconia is an amphoteric material, which means it has both acid and base sites on its surface [19]. The acid amounts of Na-ZrO_2 and ZrO_2 were estimated using NH_3-TPD analysis (Fig. 8 and Table 3). The weight-specific total acid amount was similar between Na-ZrO_2 (0.34 mmol NH_3 g^{-1}) and ZrO_2 (0.33 mmol NH_3 g^{-1}), but the area-specific acid density of Na-ZrO_2 (1.8 μmol NH_3 m^{-2}) was much smaller than that of ZrO_2 (9.7 μmol NH_3 m^{-2}). In the NH_3-TPD data (Fig. 8), NH_3 release from Na-ZrO_2 became smaller than NH_3 from ZrO_2 in the high temperature regime (400–800 °C). This result could be due to the neutralization of strong acid sites by sodium ions. Conversely, Na-ZrO_2 was higher than ZrO_2 in NH_3 release in the low-temperature regime (100–300 °C), which means Na-ZrO_2 was richer than ZrO_2 in weak acid sites. The richness of weak acid sites in Na-ZrO_2 is related to the generation of oxygen vacancies accompanied by the incorporation of low-valent ions into the zirconia framework [39]. Those oxygen vacancies are electron acceptor sites and thus behave as Lewis acid sites [39]. The identity of acid sites on Na-ZrO_2 was examined using the pyridine absorption FT-IR analysis (Fig. 9). The IR bands of pyridine approximately 1604, 1575, 1488, and 1446 cm^{-1} are characteristic of Lewis acid sites of zirconia and were observed in the spectra of both Na-ZrO_2 and ZrO_2 [24]. However, Brønsted acid sites (1540 cm^{-1}) were not observed in either catalyst. The result confirms that both catalysts had only Lewis acid sites.

Finally, when comparing the wide-angle XRD result of the *used* Na-ZrO_2 catalyst with that of *fresh* one (Fig. 4), there was no

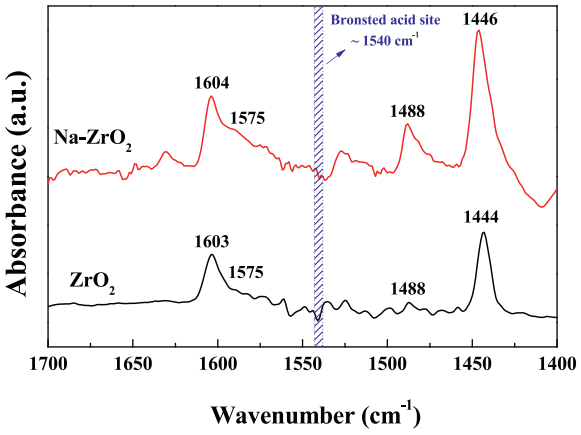

Fig. 9. FT-IR spectra of adsorbed pyridine for ZrO_2 and Na-ZrO_2 catalysts.

Table 2
Volume fractions of the monoclinic phases and the crystallite size of the ZrO_2 (*fresh*) and Na-ZrO_2 (*fresh and used*) catalysts.

Catalysts	ZrO_2 (*fresh*)	Na-ZrO_2 (*fresh*)	Na-ZrO_2 (*used*)
Volume fractions of monoclinic phases (%)	95.4	0	0
Crystallite size by Scherrer's equation (nm)	15.1	5.4	5.9

noticeable change in the XRD pattern. The Na-ZrO_2 catalyst still exhibited a diffraction pattern of pure tetragonal zirconia after being used in the reaction test. This result indicates that the tetragonal zirconia phase was stable and did not transform into the monoclinic phase during the reaction in supercritical water (400 °C, 20 bar). Meanwhile, the peak intensities decreased after reaction tests, but which did not accompany peak broadening: the FWHM value of I_t (1 0 1) peak (at $2\theta = 30.1°$) rather decreased slightly from 1.52° to 1.38°, which means the crystallite size (tetragonal zirconia) slightly increased from 5.4 to 5.9 nm after reaction test (Table 2).

3.2. Catalytic activities of ZrO_2 and Na-ZrO_2 for the conversion of PPE in supercritical water

The supercritical-water decomposition of PPE using zirconia catalysts yielded various products. Ethyl benzene, styrene and phenol were the most abundant according to product yield. These three products will be handled as *major products* hereafter. Other minor products were only found in trace amounts. These products included benzoic acid; (1-methylethyl) benzene; 1,1′-(1-methyl-1,3-propanediyl) bis-benzene; 2-(1-phenylethyl)-phenol; 4-(phenylmethyl)-phenol and (2-hydroxyphenyl) phenylmethanone, *etc.*

Fig. 10 shows the time-dependent activity of ZrO_2 catalyst. PPE conversion increased almost linearly with respect to reaction time, reaching 73% at 1.5 h. The yields of major products also increased continuously with time. The increase of phenol yield was noticeable; it increased up to 13% at 1.5 h. At 2 h, the increase in PPE conversion was slowed, and the major product yields decreased drastically (all less than 3%). Meanwhile, the production of minor products increased continuously with reaction time (not shown here).

Fig. 11 is the activity test result of the Na-ZrO_2 catalyst. Compared with the previous result using ZrO_2, conversions and yields

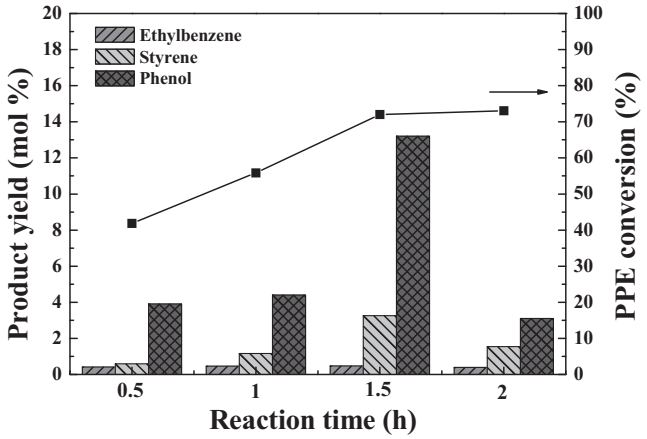

Fig. 10. PPE conversion and product yields of the ZrO_2 catalyst: reaction conditions: 4 ml of DI water; 2.5 wt.% PPE; 20 bar H_2 (initial pressure); 400 °C; 0.5–2 h; 2.5 wt.% catalyst.

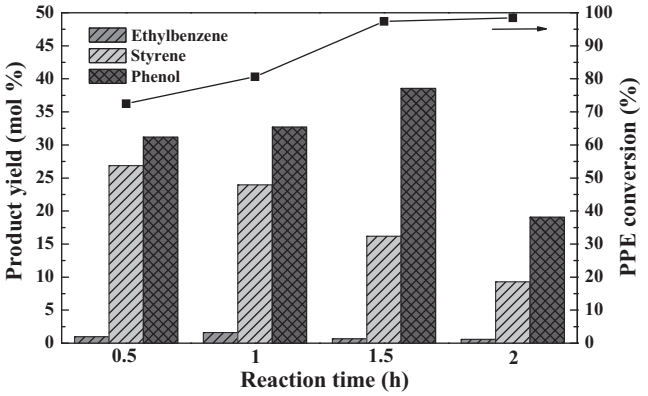

Fig. 11. PPE conversion and product yields of the Na-ZrO_2 catalyst: reaction conditions: 4 ml of DI water; 2.5 wt.% PPE; 20 bar H_2 (initial pressure); 400 °C; 0.5–2 h; 2.5 wt.% catalyst.

greatly improved. PPE conversion started with 73% at 0.5 h and increased up to 97% at 1.5 h. Phenol still had the highest yield among the products; it increased from 31 to 39% during the hour-period between 0.5 and 1.5 h. Likewise with the ZrO_2 case, the phenol yield decreased at 2 h. The styrene yield was also improved by use of the Na-ZrO_2 catalyst. At 0.5 h, it marked the highest value (27%), which was comparable to the phenol yield (31%) at the same time. However, the styrene yield continuously decreased from then on and fell down to 9% at 2 h. This result implies that styrene was consumed as an intermediate species to form other products. Styrene could be hydrogenated to ethyl benzene, but the ethyl benzene yield changed little along the reaction time. Additionally, the decrease in styrene and ethyl benzene yields did not quantitatively match the increasing phenol yield. Thus, it is expected that styrene (including the fraction converted to ethyl benzene and phenol) was converted to minor products over the course of the reaction.

3.3. Reaction mechanisms and discussions

In our previous study, it was shown that the dissociation of PPE's *β-ether* bond occurs *via* acid and base-catalyzed routes under hydrogen-pressurized high-temperature water conditions [16]. Hence, it is feasible to assume that Na-ZrO_2 and ZrO_2, both of which have been shown to be amphoteric by CO_2 and NH_3 TPD analyses, behave as acid and base catalysts simultaneously during PPE hydrolysis under supercritical water conditions. On the basis of reaction results, the acid- and base-catalyzed mechanisms to

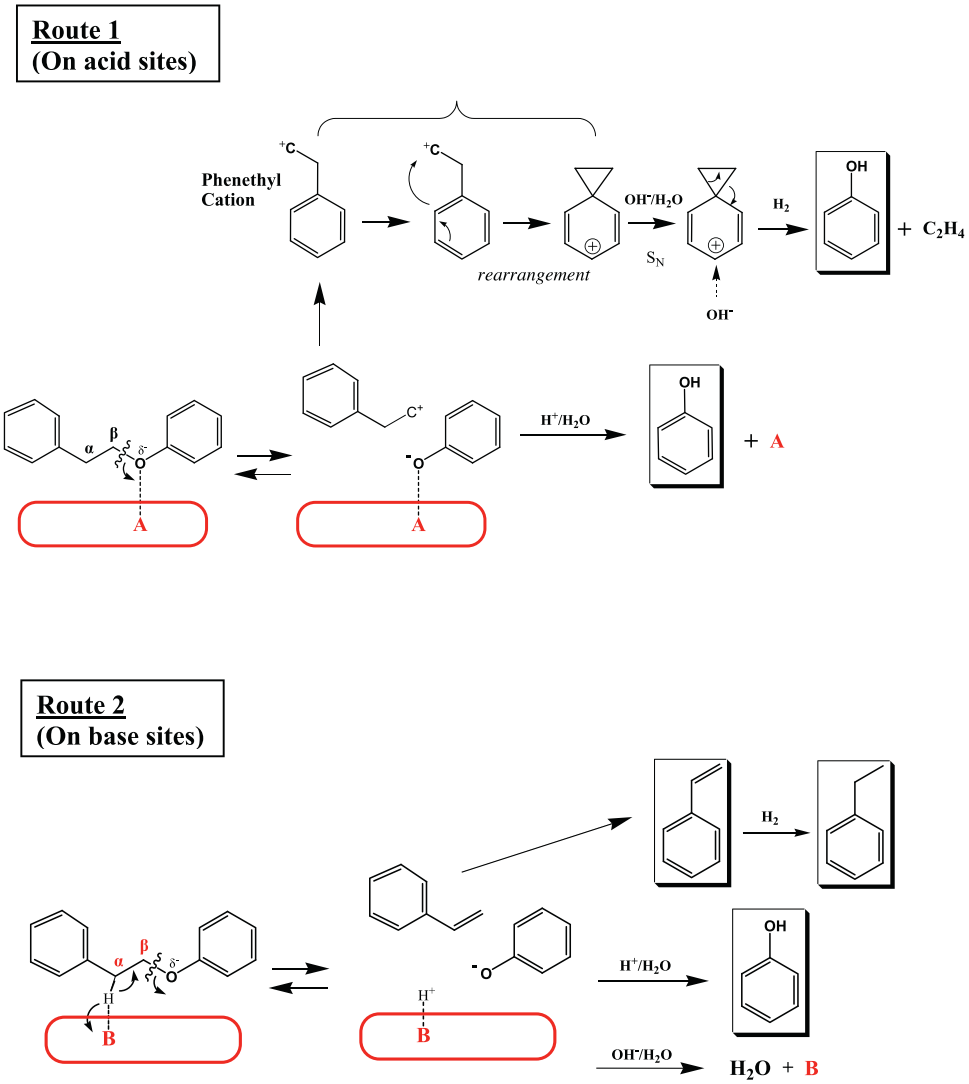

Fig. 12. The reaction mechanisms postulated for PPE hydrolysis on acid (Route 1) and base (Route 2) sites of the Na-ZrO_2 and ZrO_2 catalysts. 'A' and 'B' represent the acid and base sites of the catalysts. The boxed phenyl species indicate the primary products obtained from the route.

Table 3
Acid and base properties of ZrO_2 and Na-ZrO_2 catalysts.

Catalysts	ZrO_2	Na-ZrO_2
Total amount of base sites (mmol CO_2 g^{-1}) [a]	0.86	3.58
Density of base sites (μmol CO_2 m^{-2}) [b]	14.7	19.2
Total amount of acid sites (mmol NH_3 g^{-1}) [a]	0.34	0.33
Density of acid sites (μmol NH_3 m^{-2}) [b]	9.7	1.8

[a] Total amount of acid (base) sites was calculated as the mmols of NH_3 (CO_2) desorbed per gram of catalyst from 100 to 800 °C (35–800 °C) in NH_3-TPD (CO_2-TPD) result.
[b] Density of acid (base) sites was calculated by multiplying total amount of acid (base) site with specific surface area.

form major products (*i.e.*, phenol, styrene and ethyl benzene) over a zirconia catalyst were postulated as shown in Fig. 12.

The acid-catalyzed route ('Route 1' in Fig. 12) starts with the adsorption of PPE's electronegative oxygen to a Lewis acid site ('A' in the figure) on the zirconia catalyst. The strong O—A interaction promotes ether-bond cleavage, which produces a phenethyl cation and an adsorbed phenoxide as a result. Because the phenyl cation is not a π-LUMO acid, its direct hydrogenation to ethyl benzene is not available [16]. Instead, it rearranges and stabilizes to form a phenonium cation, which is then converted into phenol *via* nucleophilic substitution with the hydroxide anion present in the water phase. Meanwhile, the phenoxide adsorbed on the acid site turns into phenol *via* substitution with a proton present in the water phase. Thus, it could be postulated that phenol would be dominant among major products if PPE were dissociated over the acid sites of the zirconia catalyst.

In the base-catalyzed route ('Route 2' in Fig. 12), one of the *α-hydrogens* of PPE, which are the most acidic among the hydrogen atoms of PPE, is abstracted by a basic site ('B' in the figure) on the catalyst. The reaction yields styrene and the phenoxide anion. Ethyl benzene and phenol can be produced by hydrogenation of styrene and protonation of the phenoxide anion, respectively. It could be postulated that the dissociation of PPE over the base sites of Na-ZrO_2 or ZrO_2 would result in the equimolar production of phenol and styrene (+ethyl benzene).

Examining the reaction results (Fig. 11), Na-ZrO_2 produced an approximately equimolar product mixture composed of phenol and styrene (+ethyl benzene) during the initial period (0–0.5 h) of the reaction. As the reaction progressed further, the phenol yield increases but the styrene and ethyl benzene yields decreased continuously. It was expected that styrene and ethyl benzene were converted into minor products. Nevertheless, with the Na-ZrO_2 catalyst, the styrene and ethylbenzene yields were not so outnumbered by phenol as in the case of ZrO_2 catalyst (Fig. 10). Through matching the reaction results with postulated mechanisms, it is suspected that the base-catalyzed route predominates over the acid-catalyzed route in the catalysis of Na-ZrO_2 because the yields of phenol and styrene (+ethyl benzene) were comparable to each other. In contrast, the yield of phenol was much higher than that of styrene (+ethyl benzene) over the entire course of the reaction when ZrO_2 was used as the catalyst (Fig. 10). As discussed below, it is likely that the acid- and base-catalyzed routes were properly mixed during ZrO_2 catalysis.

The difference between the two catalysts' reaction mechanisms could be understood by matching the reaction results with the acid and base site concentrations on the catalysts. Whether comparing on a weight- or area-specific basis, the base sites was far richer than the acid sites on Na-ZrO_2, while the acid and base sites were relatively comparable to each other on ZrO_2 (Table 3). These site concentration results match well with the reaction results and the postulated mechanisms of the catalysts: the Na-ZrO_2 catalyst, which was far richer in base sites, was more inclined to undergo the base-catalyzed route and consequently produced phenol and styrene (+ethyl benzene) in comparable amounts. The ZrO_2 catalyst, which was relatively balanced in concentrations of acid and base sites, was simultaneously active *via* both the acid- and base-catalyzed routes. Because phenol is produced from both routes, it was produced in greater yields than both styrene and ethyl benzene.

4. Conclusion

ZrO_2 was synthesized *via* the sol-gel method, using zirconium (IV) *n*-propoxide as a precursor and Pluric P123 as a dispersant (or surfactant). The calcination of product at 500 °C (for 5 h) resulted in the formation of a monoclinic-phase-rich crystalline mixture (V_m = 95%), which showed non-porous or macroporous behavior in N_2 adsorption–desorption analysis. After post-treating with aqueous NaOH, the crystalline phase of zirconia changed into a pure tetragonal phase. Despite being obtained through the same calcination procedure with ZrO_2, Na-ZrO_2 exhibited mesoporosity (D_{BJH} = 3.1 nm), which enhanced the specific surface area (58.4 → 186.1 m^2 g^{-1}) and crystallite size (15.1 → 5.4 nm). Post-treatment with aqueous NaOH solution also influenced the acid/base properties of zirconia: untreated ZrO_2 was balanced to some degree in acid and base site concentrations, while Na-ZrO_2 was predominantly basic. All of the acid sites on ZrO_2 and Na-ZrO_2 were Lewis acids. Upon post-treatment with aqueous NaOH solution, the concentration of strong acid sites decreased, while the weak acid sites increased.

In reaction tests under conditions with supercritical water, both ZrO_2 and Na-ZrO_2 catalysts effectively cleaved PPE's *β-ether* bond to produce ethyl benzene, styrene and phenol as the major products. Overall, Na-ZrO_2 was superior to ZrO_2 in activity. Na-ZrO_2 provided yields of 39% phenol and 16% styrene with 97% PPE hydrolysis. Na-ZrO_2 was found to maintain its tetragonal phase after the reaction test.

It was supposed that Na-ZrO_2 catalyzed the reaction along the base-catalyzed route: The acidic *α-hydrogen* of PPE was abstracted with the basic sites of Na-ZrO_2, leading to the production of phenol, styrene and ethyl benzene. Separately, the acid and base site densities were comparable in the ZrO_2 catalyst. As a result, this catalyst could theoretically catalyze the reaction along both the acid- and base-catalyzed routes. The Lewis acid site on ZrO_2 captures the nucleophilic oxygen of PPE, which leads to heterolytic ether-bond cleavage producing two moles of phenol from a mole of PPE. Adding the acid-catalyzed route might enable the predominance of phenol in the reaction catalyzed by ZrO_2 catalyst.

Finally, it was supposed that the higher activity of Na-ZrO_2 compared with ZrO_2 is attributed to the textural properties (specific surface area, crystallite size) and base site concentration, both of which were enhanced by the NaOH solution post-treatment.

Acknowledgment

This work was supported by the MSIP (Ministry of Science, ICT & Future Planning) of Korea Grant funded by the Korean Government (NRF-2012R1A2A1A03009667).

References

[1] S.H. Kim, C.M. Lee, K. Kafle, Korean J. Chem. Eng. 30 (12) (2013) 2127–2141.
[2] W. Boerjan, J. Ralph, M. Bauer, Annu. Rev. Plant Biol. 54 (1) (2003) 519–549.
[3] T.H. Kim, Korean J. Chem. Eng. 29 (1) (2012) 82–88.
[4] R. Ravikumar, B.V. Ranganathan, K.N. Chathoth, S. Gobikrishnan, Korean J. Chem. Eng. 30 (5) (2013) 1051–1057.
[5] M. Wahyudiono, M. Sasaki, Goto, Chem. Eng. Process.: Process. Intensif. 47 (2008) 1609–1619.
[6] A.O. Ayeni, J.A. Omoleye, S. Mudliar, F.K. Hymore, R.A. Pandey, Korean J. Chem. Eng. 31 (7) (2014) 1180–1186.

[7] J. Zakzeski, P.C.A. Bruijnincx, A.L. Jongerius, B.M. Weckhuysen, Chem. Rev. 110 (2010) 3552–3599.
[8] M.P. Pandey, C.S. Kim, Chem. Eng. Technol. 34 (1) (2011) 29–41.
[9] S. Kangm, X. Li, J. Fan, J. Chang, Renew. Sustain. Energy Rev. 27 (2013) 546–558.
[10] C. Amen-Chen, H. Pakdel, C. Roy, Bioresour. Technol. 79 (2001) 277–299.
[11] H.W. Park, J.K. Kim, U.G. Hong, Y.J. Lee, J.H. Song, I.K. Song, Catal. Surv. Asia 17 (2013) 119–131.
[12] X. Chen, N. Yan, Catal. Surv. Asia (2015), http://dx.doi.org/10.1007/s10563-014-9171-1 (in press).
[13] Q. Song, J. Cai, J. Zhang, W. Yu, F. Wang, J. Xu, Chin. J. Catal. 34 (2013) 651–658.
[14] A. Beste, A.C. Buchanan III, Chem. Phys. Lett. 550 (2012) 19–24.
[15] H.W. Park, S. Park, D.R. Park, J.H. Choi, I.K. Song, J. Ind. Eng. Chem. 174 (2011) 736–741.
[16] H.-J. Eom, D.-W. Lee, Y.-K. Hong, S.-H. Chung, M.-G. Seo, K.-Y. Lee, Appl. Catal. A: Gen. 472 (2014) 152–159.
[17] S. Liu, S. Huang, L. Guan, J. Li, N. Zhao, W. Wei, Y. Sun, Microporous Mesoporous Mater. 102 (2007) 304–309.
[18] A.A. Clifford, in: E. Kiran, P.G. Debenedetti, C.J. Peters (Eds.), Supercritical Fluids: Fundamentals and Applications, Kluwer Academic Publishers, The Netherlands, 1994, p. 455.
[19] H. Hattori, Chem. Rev. 95 (1995) 537–558.
[20] D.-W. Lee, Y.-M. Park, K.-Y. Lee, Catal. Surv. Asia 13 (2009) 63–77.
[21] M. Watanabe, H. Inomata, M. Osada, T. Sato, T. Adschiri, K. Arai, Fuel 82 (2003) 545–552.
[22] M. Watanabe, Y. Aizawa, T. Iida, R. Nishimura, H. Inomata, Appl. Catal. A: Gen. 295 (2005) 150–156.
[23] H. Wang, M. Wang, N. Zhao, W. Wei, Y. Sun, Catal. Lett. 105 (2005) 253–257.
[24] M.E. Manríquez, T. López, R. Gómez, J. Navarrete, J. Mol. Catal. A: Chem. 220 (2004) 229–237.
[25] T. Yamaguchi, Catal. Today 20 (1994) 199–217.
[26] K.T. Jungm, Y.G. Shul, A.T. Bell, Korean J. Chem. Eng. 18 (6) (2001) 992–999.
[27] R. Marcus, U. Diebold, R.D. Gonzalez, Catal. Lett. 86 (2003) 151–156.
[28] M.K. Mishra, B. Tyagi, R.V. Jasra, J. Mol. Catal. A: Chem. 223 (2004) 61–64.
[29] H. Eltejaei, J. Towfighi, H.R. Bozorgzadeh, M.R. Omidkhah, A. Zamaniyan, Mater. Lett. 65 (2011) 2913–2916.
[30] S. Liu, J. Ma, L. Guan, J. Li, W. Wei, Y. Sun, Microporous Mesoporous Mater. 117 (2009) 466–471.
[31] K. Cassiers, T. Linssen, V. Meynen, P. Van Der Voort, P. Cool, E.F. Vansant, Chem. Commun. 10 (2003) 1178–1179.
[32] D.K. Johnson, H.L. Chum, R. Anzick, R.M. Baldwin, Research in Thermochemical Biomass Conversion, Elsevier Applied Science, New York, 1988, pp. 485–496.
[33] M. Osada, T. Sato, M. Watanabe, T. Adschiri, K. Arai, Energy Fuels 18 (2) (2004) 327–333.
[34] V.G. Deshmane, Y.G. Adewuyi, Microporous Mesoporous Mater. 148 (2012) 88–100.
[35] S.-W. Cao, Y.-J. Zhu, J. Wu, K.-W. Wang, Q.-L. Tang, Nanoscale Res. Lett. 5 (2010) 781–785.
[36] K. Cassiers, T. Linssen, K. Aerts, P. Cool, O. Lebedev, G. Van Tendeloo, R.V. Grieken, E.F. Vansant, J. Mater. Chem. 13 (2003) 3033–3039.
[37] S.G. Liu, H. Wang, J.P. Li, N. Zhao, W. Wei, Y.H. Sun, Mater. Res. Bull. 42 (2007) 171–176.
[38] K. Pokrovski, K.T. Jung, A.T. Bell, Langmuir 17 (2001) 4297–4303.
[39] H. Teterycz, R. Klimkiewicz, M. Łaniecki, Appl. Catal. A: Gen. 249 (2003) 313–326.